AIAA JOURNAL
Vol. 50, No. 10, October 2012

Wall-Pressure Spectral Model Including the Adverse Pressure Gradient Effects

Yannick Rozenberg* and Gilles Robert†
École Centrale de Lyon, 69134 Écully, France
and
Stéphane Moreau‡
Université de Sherbrooke, Sherbrooke, Quebec J1K 2R1, Canada

DOI: 10.2514/1.J051500

An empirical model to predict the wall-pressure fluctuation spectra beneath adverse pressure gradient flows is presented. It is based on Goody's model, which already incorporates the effect of Reynolds number but is limited to zero pressure gradient flows. The extension relies on six test cases from five experimental or numerical studies covering a large range of Reynolds number, $5.6 \times 10^2 < R_\theta < 1.72 \times 10^4$, in both internal (channel) and external (airfoil) flows. A review of the boundary-layer parameters characterizing the pressure gradient effects is provided, and the more relevant ones are introduced as new variables in the model. The method is then compared to the zero pressure gradient model it is derived from. The influence of the pressure gradient on the wall-pressure spectrum is discussed. Finally, the method is applied to provide input data of a radiated trailing-edge noise model by means of an aeroacoustic analogy, namely Amiet's theory of turbulent boundary layer past a trailing edge. The results are compared to experimental data obtained in an open-jet anechoic wind tunnel.

Nomenclature

b	=	Corcos's constant
C_1, C_2, C_3	=	Goody's model constants
C_f	=	skin friction coefficient
C_p	=	pressure coefficient
C^+	=	constant in the log law
c_0	=	speed of sound, $\mathrm{m} \cdot \mathrm{s}^{-1}$
g	=	wall-law function
$H = \delta^*/\theta$	=	shape factor
h	=	Cole's wake-law function
k	=	wavenumber, m^{-1}
l_y	=	coherence spanwise length scale, m
p	=	pressure, Pa
$\bar{p}^2$	=	mean square unsteady pressure, Pa^2
R_T	=	ratio of timescales of pressure
R_θ	=	Reynolds number based on U_e and θ
U_c	=	convection velocity, $\mathrm{m} \cdot \mathrm{s}^{-1}$
U_e	=	external velocity $\mathrm{m} \cdot \mathrm{s}^{-1}$
U_i	=	inlet velocity $\mathrm{m} \cdot \mathrm{s}^{-1}$
u_τ	=	friction velocity $\mathrm{m} \cdot \mathrm{s}^{-1}$
β_C	=	Clauser's parameter
Δ	=	Zagarola and Smits's parameter
δ	=	boundary-layer thickness, m
δ^*	=	boundary-layer displacement thickness, m
θ	=	boundary-layer momentum thickness, m
κ	=	von Kármán constant
ν	=	kinematic viscosity, $\mathrm{s}^2 \cdot \mathrm{m}^{-2}$
Π	=	wake strength parameter
ρ_0	=	air density, $\mathrm{kg} \cdot \mathrm{m}^{-3}$
τ_w	=	wall shear stress, Pa
$\tau_{\max}$	=	maximum shear stress, Pa
ω	=	angular frequency
$\tilde{\omega}$	=	Strouhal number based on external variables
Φ_{pp}	=	power spectral density of surface pressure fluctuations, $\mathrm{Pa}^2/\mathrm{Hz}$
$\bar{\ }$	=	mean value

Received 15 July 2011; revision received 13 February 2012; accepted for publication 3 March 2012.

*Research Engineer, Laboratoire de Mécanique des Fluides et d'Acoustique, UMR CNRS 5509; currently Assistant Professor, Université Lyon 1, 43 Boulevard du 11 Novembre 1918, 69622 Villeurbanne Cedex; yannick.rozenberg@ec-lyon.fr.

†Assistant Professor, Laboratoire de Mécanique des Fluides et d'Acoustique, UMR CNRS 5509; gilles.robert@ec-lyon.fr.

‡Professor, Mechanical Engineering Department, Groupe d'Acoustique de l'Université de Sherbrooke; stephane.moreau@usherbrooke.ca.

I. Introduction

WALL-PRESSURE fluctuations induced by flow over a solid surface result from turbulent velocity fluctuations in the turbulent boundary layer. Studying and modeling them is of fundamental and practical interest. The diffraction of wall-pressure fluctuations near edges yields the so-called trailing-edge noise [1–4], which constitutes the most basic aeroacoustic mechanism of a surface of limited extent embedded in a clean flow. Likewise, the vibration of a panel induced by the pressure fluctuations leads to the generation of acoustic radiation into an aircraft cabin, for example, and the knowledge of the wall-pressure statistics is required to evaluate the passenger disturbance during the flight. Taking the divergence of the incompressible Navier–Stokes equations and performing a Reynolds decomposition leads to the following Poisson's equation that relates the pressure fluctuations p to the fluctuating velocity u_i and the mean velocity U_i:

$$\frac{1}{\rho}\frac{\partial^2 p}{\partial x_i^2} = 2\frac{\partial \bar{U}_i}{\partial x_j}\frac{\partial u_j}{\partial x_i} - \frac{\partial^2 (u_i u_j - \bar{u}_i \bar{u}_j)}{\partial x_i \partial x_j} \tag{1}$$

As noted by Bull [5], the integral solution of this equation implies that the pressure is determined by contributions from all parts of the velocity field. Because there is no universal law to describe the velocity field in the different layers of the boundary layer, because the turbulent eddies are convected at different velocities depending on their distance to the wall, and because the wall pressure is influenced by the velocity fluctuations in the whole boundary layer, the pressure field structure is inevitably complex. Accurate predictions of such pressure fields have been performed, using direct numerical simulations or large-eddy simulations [6–8]. Such computations are highly time-consuming and not yet affordable in complex

configurations. In such cases, the flowfield is often determined by Reynolds-averaged Navier–Stokes (RANS) simulations. Adequate postprocessing coupled with statistical models has been used to determine the pressure autospectrum.

Lee et al. [9] developed a spectral modeling scheme coupled with a RANS simulation. The vertical turbulent fluctuating velocity and the gradients of the streamwise mean shear velocity were predicted from the turbulent kinetic energy. The model was then applied to an equilibrium flow with fairly good agreement. It has been extended to nonequilibrium flows by adding a nonlinear source term in the Poisson equation [10]. Based on the same idea of modeling the space–time velocity correlation using RANS data, Peltier and Hambric [11] proposed a stochastic model to predict wall-pressure spectra. The effects of pressure gradients (favorable, zero, and adverse) are correctly predicted, but the validation is limited to mild pressure gradients. Recently, Remmler et al. [12] readdress the modeling of wall-pressure spectra on the basis of Panton and Linebarger's hypotheses [13] as well as input data from steady RANS simulations. The far-field acoustic pressure radiated by a highly loaded airfoil is then favorably compared with experimental data.

Another technique to predict wall-pressure spectra is a scaling that consists in the use of appropriate normalized parameters to collapse wall-pressure spectra on a single curve. Unfortunately, there is no universal scaling that collapses the pressure spectra for a large frequency range and different Reynolds numbers. For zero pressure gradient flows, various models and normalized parameters have been proposed. The present paper aims to extend this technique to adverse pressure gradient (APG) flows, such as canonical channel flows or more realistic flows around airfoils with positive angle of attack. In Sec. II, three empirical models relying on theoretical and experimental studies are reviewed. They are limited to zero pressure gradient (ZPG) flows and underestimate the wall-pressure spectrum in APG configurations. Then, the effects of the APG on the turbulent boundary layer parameters are studied in Sec. III, and the more relevant parameters, characterizing the boundary layer and its history, are selected. The proposed model, based on Goody's model [14] and taking into account the APG effects, is presented in Sec. IV and assessed in Sec. V.

II. Review of Empirical Wall-Pressure Spectral Models

The turbulent boundary layer is characterized by a large range of relevant length, velocity, and pressure scales. A two-layer model is widely used to scale the turbulent boundary layer. The nearest flow to the wall, called the viscous sublayer, provides a first set of length, velocity, and pressure scales; the outer layer provides a second one. Based on this description, Keith et al. [15] compared the wall-pressure spectra from various experiments corrected for spatial resolution errors [16] in a normalized form. The high-frequency range of the pressure spectra collapses when it is normalized by inner-layer scales, such as the wall shear stress τ_w for the pressure scale and ν/u_τ^2 for the timescale, with ν as the kinematic viscosity and u_τ as the friction velocity. For low frequencies, a collapse is observed with outer-layer scaling, such as the velocity at the boundary layer edge U_e, the boundary-layer thickness δ, or the boundary-layer displacement thickness δ^*. Based on this description, three empirical wall-pressure spectral (WPS) models are briefly reviewed: Amiet's model, Chase–Howe's model, and Goody's model. The latter takes into account the effect of the Reynolds number. For a more detailed review of semi-empirical models for turbulent boundary layer wall-pressure spectra, the reader is invited to refer to the paper by Hwang et al. [17]. The wall-pressure spectra presented in the present article follow the single-sided convention: $\bar{p}^2 = \int_0^\infty \Phi_{pp}(\omega)\,\mathrm{d}\omega$.

A. Amiet's WPS Model

Willmarth and Roos [18] have collected experimental wall-pressure fluctuations beneath a turbulent boundary layer. Based on these data, Amiet [1] proposed an analytical formulation using the outer variables:

$$\frac{\Phi_{pp}(\omega)}{\rho_0^2 \delta * U_e^3} = 2.10^{-5}\frac{F(\tilde{\omega})}{2} \tag{2}$$

where

$$F(\tilde{\omega}) = (1 + \tilde{\omega} + 0.217\tilde{\omega}^2 + 0.00562\tilde{\omega}^4)^{-1}$$

with $\tilde{\omega} = \omega\delta^*/U_e$ and $0.1 < \tilde{\omega} < 20$.

Figure 1 compares the model with data collected by Keith et al. [15] and scaled by outer variables. It represents a good mean value, but the data are spread out, in particular at high frequencies. At low frequencies, data collapse except Choi and Moin's. It is to be noted that the latter are the only ones coming from a numerical simulation at a low Reynolds number $R_\theta = 1332$ based on the external velocity and the momentum thickness.

B. Chase–Howe's WPS Model

Based on the theoretical model developed by Chase [28], Howe describes the spectral behavior of the wall-pressure field at low Mach number in the convective domain, namely for $k \gg \omega/c_0$ [29]. Based on mixed variables, Howe suggests the following formulation:

$$\frac{\Phi_{pp}(\omega)U_e}{\tau_w^2\delta^*} = \frac{2\tilde{\omega}^2}{[\tilde{\omega}^2 + 0.0144]^{3/2}} \tag{3}$$

As observed by Keith et al. [15], the use of mixed variables to define a scaling law is worthwhile because the data have a better collapse than with outer variables. Experimental wall-pressure spectra exhibit three slopes: a positive slope at low frequencies, a slight negative slope in the overlap region, and a high negative slope at high frequencies. The Chase–Howe spectrum is proportional to ω^2 at low frequencies. It varies as ω^{-1} at higher frequencies, corresponding to the wall-pressure spectra behavior in the overlap region where both inner- and outer-layer scaling can be used to make the data collapse [30]. However, it does not include the third slope at higher frequencies as experimentally and theoretically observed (cf. Fig. 2).

C. Goody's WPS Model

The discrepancies observed at high frequencies in Fig. 2 are attributed to Reynolds number effects. Goody's objective is to take into account this effect of the Reynolds number using an empirical approach [14]. Based on Chase–Howe's model and the experimental results of seven research teams, he modified Eq. (3) to agree better with the experimental data. A term was added to the denominator so that spectral levels decay as ω^{-5} when $\omega \to \infty$. The exponents in the denominator were changed to better agree with the measured pressure spectral behavior in the overlap range (middle frequencies with a $\omega^{-0.7}$ decay). Moreover, the only effect of Reynolds number on the shape of the wall-pressure spectrum is to increase the size of the overlap range. Finally, δ is preferred to δ^* because the largest coherent structures are in the order of δ. The final form of the semi-empirical model is

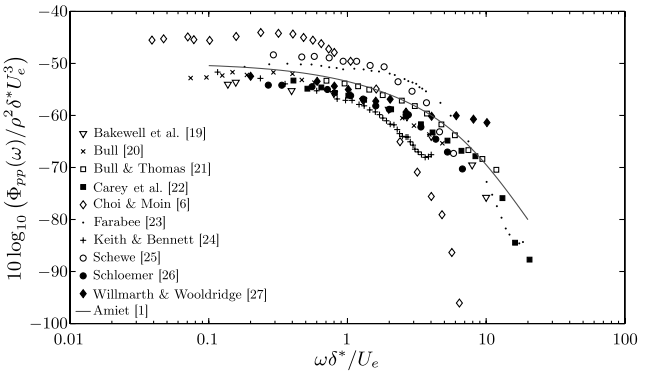

Fig. 1 Wall-pressure spectra scaled by outer variables. Amiet's WPS model [1] vs data collected by Keith et al. [15] and corrected for spatial resolution errors.

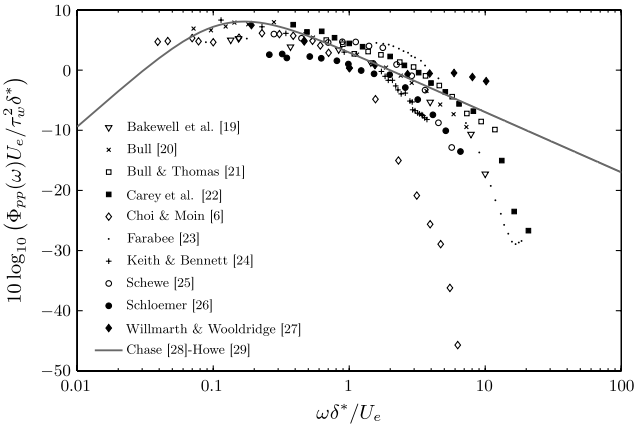

Fig. 2 Wall-pressure spectra scaled by mixed variables. Chase–Howe [28,29] model vs data collected by Keith et al. [15] and corrected for spatial resolution errors.

$$\frac{\Phi_{pp}(\omega)U_e}{\tau_w^2\delta} = \frac{C_2(\omega\delta/U_e)^2}{\left[(\omega\delta/U_e)^{0.75}+C_1\right]^{3.7}+[C_3(\omega\delta/U_e)]^7} \tag{4}$$

where C_1, C_2, and C_3 are empirical constants with the following recommended value: 0.5, 3.0, and $1.1R_T^{-0.57}$, respectively, with $R_T = (\delta/U_e)/(\nu/u_\tau^2) = (u_\tau\delta/\nu)\sqrt{C_f/2}$ as the ratio of the outer to inner boundary layer time scale.

Hwang et al. concluded in their review of empirical wall-pressure spectral models [17] that Goody's model shows the best agreement with experiments. Goody has captured the spectral features correctly for zero pressure gradient turbulent boundary layer flows over a wide range of Reynolds number. As observed in Fig. 3, the discrepancies at high frequencies are related to the ratio of outer layer to inner layer timescale R_T, and the cutoff frequency is well predicted. Nevertheless, the model is limited to canonical flows, such as pipe flow and turbulent boundary layer over flat plate.

III. Adverse Pressure Gradient Effects on the Turbulent Boundary Layer

In many applications, the turbulent boundary layer encounters an adverse mean-pressure gradient. This is the case, for example, on the suction side of a profile or a blade, just upstream of the trailing edge. The spectrum of the wall-pressure fluctuations at this position is of practical interest for trailing-edge noise prediction using analytical models, as long as the boundary layer remains attached. Empirical models reviewed in Sec. II are no longer suited to such flows. In the following section, the effects of the adverse pressure gradient on pressure fluctuations statistics are presented, and six reference spectra from five numerical and/or experimental studies are selected to find some parameters characterizing the pressure-gradient effects and the boundary layer history, to add an APG effect into Goody's model.

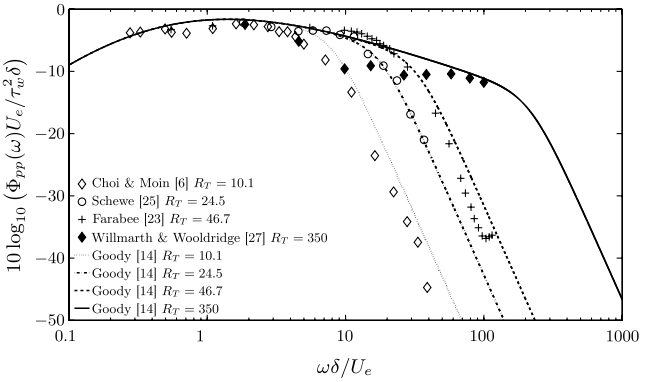

Fig. 3 Wall-pressure spectra scaled by mixed variables. Goody's model [14] vs data collected by Keith et al. [15] and corrected for spatial resolution errors.

A. Effects on the Pressure Statistics

In 1967, Schloemer [26] experimentally observed the strong effect of the mean-pressure gradient on the wall-pressure fluctuations. Spectral levels were increased for positive pressure gradient boundary layers. This is not only caused by the thickening of the boundary layer, because this trend is also observed when the wall-pressure spectra are scaled with the boundary layer displacement thickness (cf. Fig. 4). Results obtained by Na and Moin [7] from direct numerical simulation of a pipe flow with pressure gradients, created by prescribed vertical velocity distributions along the upper boundary, are also plotted. The adverse pressure effects can lead to an increase of 10 dB at low frequency. If this effect is not taken into account in the trailing-edge noise prediction, it would lead to a dramatic underestimate of the noise, because it is directly proportional to the wall-pressure spectrum in the analytical models proposed by Howe and Amiet. To build a new empirical model, parameters that characterize pressure gradients and their influence on the wall-pressure statistics will be defined.

B. Test Cases Definition

The purpose of the present study is to propose an empirical wall-pressure spectral model using boundary-layer parameters, taking into account the adverse-pressure gradient effect. Test cases have to be fully documented to provide inner and outer boundary-layer variables and wall-pressure spectra. Such test cases are not common in the scientific literature. Five studies have been selected. Three are pipe-flow turbulent boundary layers: an experimental study by Schloemer [26], a numerical study using direct numerical simulations by Na and Moin [7] and Na [31], and experimental results [32] and RANS simulations of a pipe flow with favorable and adverse pressure gradients. Two are turbulent boundary layers on loaded profiles: experimental results [33,34] and RANS simulations on two loaded profiles.

1. *Schloemer's Data*

Using flush-mounted transducers, Schloemer [26] measured the pressure fluctuations at the bottom wall of a low-turbulence subsonic

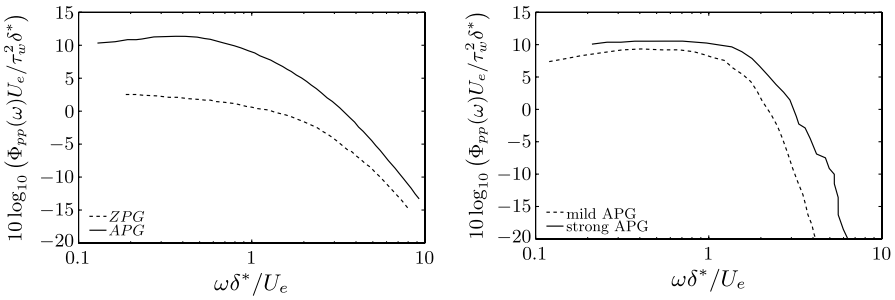

a) Schloemer [26] **b) Na [7]**

Fig. 4 Wall-pressure spectra scaled with mixed variables: APG effect.

Table 1 Inner and outer boundary-layer variables from test cases

	Pipe flows			Airfoils		
	Schloemer APG	Na Strong APG	ENABLE $x = 250$ cm	V2 airfoil RMP 17	V2 airfoil RMP 23	CD airfoil RMP 25
CFD or Exp.	Exp.	CFD	CFD	CFD	CFD	CFD
U_e, m/s	43.6	7.4	75.9	20.9	19.8	16.9
δ, m	2.56×10^{-2}	2.62×10^{-2}	2.65×10^{-2}	2.73×10^{-3}	3.87×10^{-3}	4.98×10^{-3}
δ^*, m	5.26×10^{-3}	4.1×10^{-3}	4.53×10^{-3}	6.97×10^{-4}	9.92×10^{-4}	2.24×10^{-3}
θ, m	3.33×10^{-3}	2.69×10^{-3}	3.40×10^{-3}	4.05×10^{-4}	5.59×10^{-4}	8.76×10^{-4}
$H = \delta^*/\theta$	1.58	1.52	1.33	1.72	1.77	2.55
τ_w, Pa	1.99	0.099	7.00	1.01	0.72	0.11
$\tau_{\max}$, Pa	——	——	7.40	1.06	0.75	0.167
$\beta_C = (\theta/\tau_w)(\mathrm{d}p/\mathrm{d}x)$	2.07	1.14	1.11	0.19	1.68	20.9
Π	2.15	1.37	1.09	1.03	1.59	8.18
$R_\theta = U_e\theta/\nu$	9180	1332	17,170	564	736	982
$\Delta = \delta/\delta^*$	4.86	6.39	5.84	3.92	3.90	2.23

wind-tunnel. At the top wall, a half-airfoil section was attached to obtain favorable or adverse pressure gradients at the transducer position. Mean velocity profiles were obtained by single hot-wire measurements. For a given pressure gradient, when the wall-pressure spectra was normalized by a third power of the external velocity U_e and plotted as a function of Strouhal number based on the boundary-layer displacement thickness, a good collapse was observed. The boundary-layer parameters measured by Schloemer are recalled in Table 1. They correspond to the normalized wall-pressure spectra presented in Fig. 4a.

2. *Na and Moin's Data*

Na and Moin [7] performed a direct numerical simulation of a pipe flow encountering a mean-pressure gradient and corresponding to Spalart and Watmuff's experiment [35]. Wall-pressure fluctuations were studied in detail; evolution of spectra, two-point velocity correlations, and convection velocities were extracted along the streamwise direction. Inner and outer boundary-layer parameters were given for a positive pressure gradient in Table 1.

3. *Environmental Noise Associated with Turbulent Boundary Layer Excitation*

An experimental campaign was conducted at the École Centrale de Lyon (ECL) wind tunnel to constitute an experimental database with the aerodynamic characteristics of the turbulent boundary layer and the wall-pressure fluctuations for different mean pressure gradients. The test section was a square section of 0.5 m sides and a length of 6 m along the x axis. The flow first encountered a favorable pressure gradient (FPG) and then an adverse pressure gradient (APG), as can be seen in Fig. 5, where the wall-pressure coefficient $C_p = (p - p_i)/(1/2\rho_i U_i^2)$ along the streamwise direction is plotted. Measurements were made for three inflow velocities from $U_i = 25$ m/s to $U_i = 50$ m/s, but the present study will focus on the higher-velocity case. The mean and fluctuating downstream components of the velocity were obtained by hot-wire anemometry.

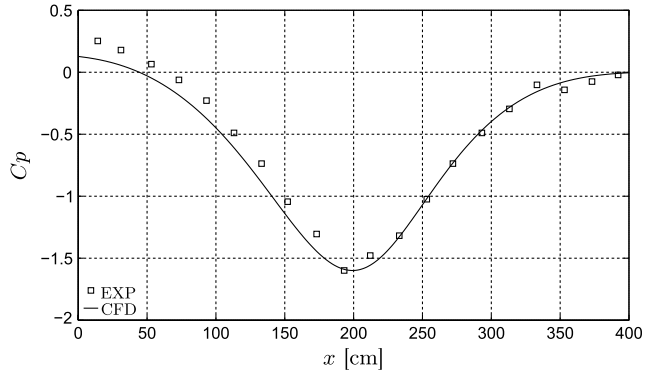

Fig. 5 Wall-pressure coefficient along the streamwise direction at the bottom side of the test section.

The wall shear stress τ_w was also measured with a Preston tube and a Weiser probe. The Weiser probe estimate was found to be 10% lower than the Preston tube estimate. The outer diameter of the Preston tube was 1 mm. The standard curve of Patel [36] was used for calibration. As the Weiser probe was calibrated in a two-dimensional pipe flow with a constant mean pressure gradient, values from the Weiser probe are kept here.

ENABLE configuration has also been simulated with Fluent 6.2 using the k–ω shear stress transport (SST) model and assuming a two-dimensional flow. The pressure distribution is well reproduced by the simulation, especially in the APG region. The velocity profiles are also compared in Fig. 6. The acceleration in the FPG region is followed by a deceleration in the APG region. In the former, the boundary-layer thickness decreases, whereas it increases in the latter. The CFD fluctuating velocity profiles have been deduced from the turbulent kinetic energy combined with an anisotropy factor based on the turbulent boundary layer data collected by Klebanoff [37]. Even though Klebanoff's data were measured for a zero pressure gradient boundary layer, the anisotropy factor used for the streamwise fluctuating velocity gives quite reliable data for a two-dimensional RANS simulation. The friction velocity is presented in Fig. 7. Values given by Fluent and based on the upwind finite-difference estimates are compared to the one deduced by the methodology proposed by Allen and Tudor [38]. A general good agreement is observed. The data are more widely spread at $x = 150$ cm and $x = 200$ cm, where disagreements of up to 10% are observed. It corresponds to the flow positions around which the pressure gradient sign changes from negative to positive. Beyond these positions, the discrepancies are less than 5% between CFD values, Allen and Tudor's technique, and experimental data obtained by the Weiser probe. The boundary-layer parameters at the location $x = 250$ cm in the APG region, given by CFD and in agreement with the experiment, are summarized in Table 1.

4. *V2 Airfoil*

The V2 airfoil is a low, subsonic profile designed for automotive engine-cooling fans. Aerodynamic and acoustic data are collected to study trailing-edge noise. The experimental setup has already been described by Moreau and Roger [34,39]. The mock-up has a chord length of 13.6 cm and a span of 30 cm. The geometry and probes locations are presented in Fig. 8a. The remote microphone probes (RMPs) allow the measurements of the mean and fluctuating pressure within the frequency range 20 Hz–25 kHz. Such a probe is made with a spanwise flush-mounted capillary tube and a pinhole at the measuring point. The capillary is progressively enlarged outside the mock-up until a small electret microphone can be flush mounted [40]. Some hot-wire velocity profiles are also collected, especially in the wake, just downstream of the trailing edge. The instrumented airfoil is placed in the ECL small wind tunnel nozzle exit (13×30 cm) at a high angle of attack ($\alpha = 20$ deg) to obtain a strong adverse pressure gradient without separation of the turbulent boundary layer. The presence of a separated flow near the trailing

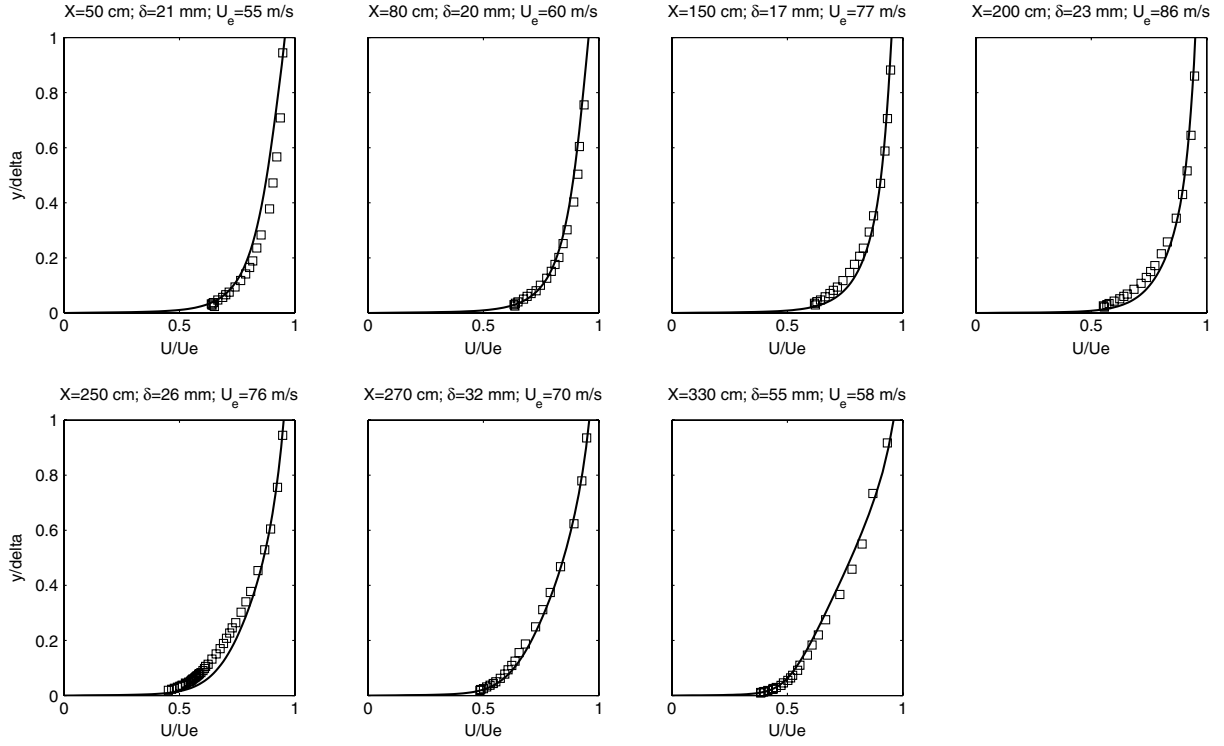

a) Mean-velocity profile

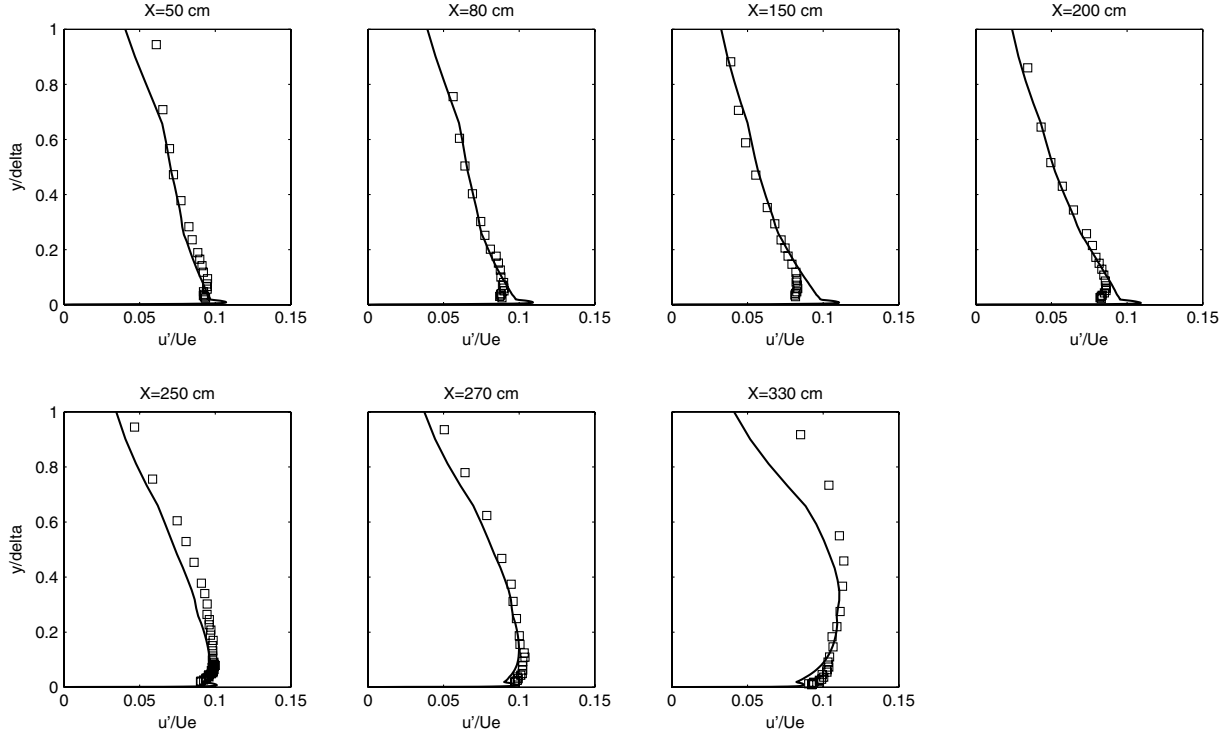

b) Fluctuating-velocity profile

Fig. 6 Mean and fluctuating velocity profiles (downstream component) along the *x* axis; experimental results—RANS computation (□).

edge is not clear because the numerical simulation does not exhibit any plateau in the mean pressure distribution, whereas the experimental results have one (cf. Fig. 9). However, the convection velocity is positive along the whole chord, suggesting an attached flow. The deflection of the jet, leading to a lower effective angle of attack than the geometric one, prevents any stall at this high angle of attack. The influence of the jet on the airfoil loading has been discussed by Moreau et al. [41].

The experimental aerodynamic data are not sufficient to provide the boundary-layer parameters needed for the normalization of wall-pressure spectra obtained in the experiment. A two-dimensional RANS simulation has been carried out using Fluent 6.2 on an unstructured grid. The nozzle of the wind tunnel and the acoustic chamber have also been simulated to account for the installation effects [41]. The grid is composed of 63,000 nodes. The mesh has been refined to obtain a dimensionless distance to the wall, y^+, smaller than 1 around the airfoil and to avoid the use of wall-functions. Because the k–ω SST model [42] was found to be well suited to low-Reynolds-number flows with adverse pressure gradients [41], it has been selected for the study. It is also well suited

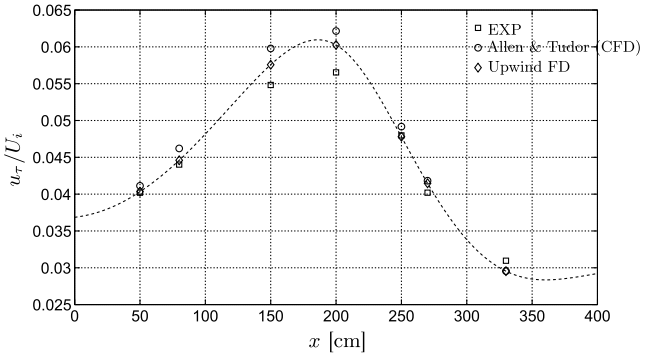

Fig. 7 Friction velocity normalized by the inlet velocity. Experimental results (Weiser probe) compared with upwind FD and Allen and Tudor's method [38].

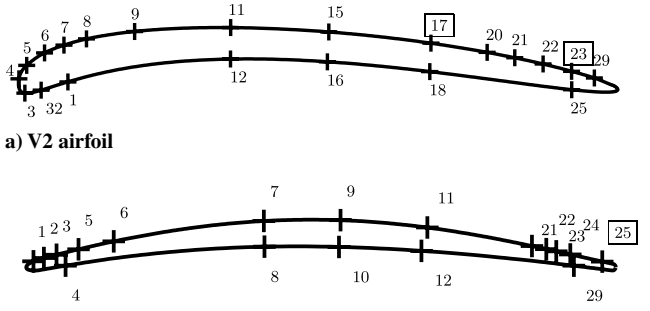

a) V2 airfoil

b) CD airfoil

Fig. 8 RMP positions on airfoils.

to capture the separation bubble near the leading edge in the boundary layer. To mimic the experimental condition, the inflow velocity is iteratively modified to obtain $U_i = 16$ m/s at the nozzle exit. To validate the simulation, three flow features have been investigated: 1) the mean-pressure distribution along the suction side, 2) the presence of the laminar separation bubble typical of low-Reynolds-number, thin airfoils, and 3) the mean velocity profile in the wake, just downstream of the trailing edge.

The comparisons between the experimental results and the simulation are presented in Figs. 9 and 10. The experimental mean wall-pressure coefficient C_p is well reproduced by the simulation, except near the leading-edge in the laminar separation bubble, which is found to be highly unsteady in the measurements. For the mean wall pressure, two campaigns have been carried out, and the error bars point out the repeatability of the measurements. The simulation captures both position and length of the laminar separation bubble correctly. Because the transition to turbulence occurs around the reattachment point of the laminar bubble, its presence in the simulation is crucial to obtain the realistic growth and development of the turbulent boundary layer toward the trailing edge. In Fig. 10, the velocity profile in the wake obtained by the steady simulation is

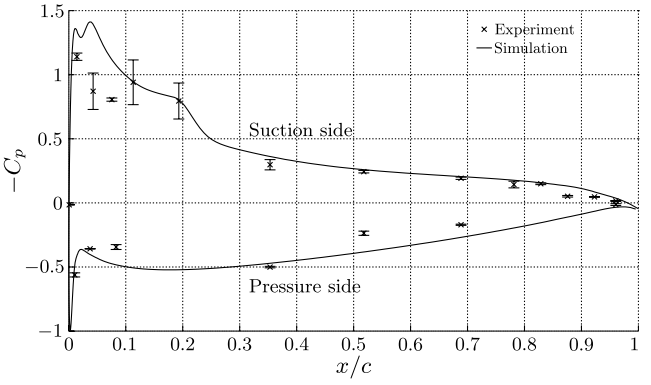

Fig. 9 Mean pressure coefficient ($-C_p$) on V2 airfoil.

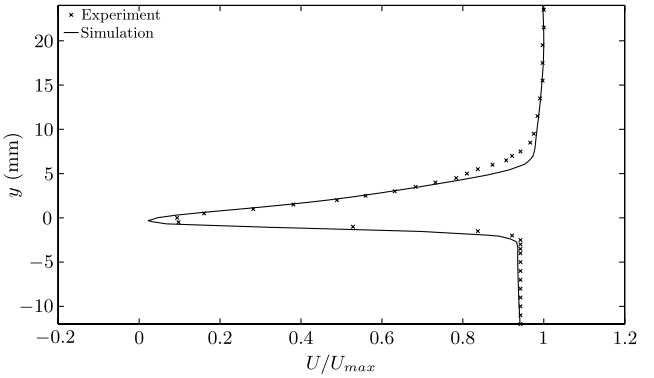

Fig. 10 Velocity profile in the wake 2 mm downstream of the trailing edge. Experimental results are obtained by single hot-wire measurements.

very close to the experimental data. Because the wake is the combination of boundary layers coming from the suction and pressure sides, the boundary layers close to the trailing edge are also likely to be correctly reproduced.

The boundary-layer velocity profiles are extracted along a direction normal to the wall, at the RMP locations on the suction side close to the trailing edge. To obtain the friction velocity u_τ, the methodology proposed by Allen and Tudor [38] is preferred to the direct upwind finite-difference estimates. The values are summarized in Table 1, for the two RMP locations studied in the next sections.

5. *Controlled-Diffusion Airfoil*

A similar configuration was studied numerically and experimentally on a low-speed controlled-diffusion (CD) airfoil [41,43]. The experimental results were obtained by Moreau and Roger [34] in the anechoic wind tunnel at ECL. The reference velocity was 16 m/s, leading to a Reynolds number based on the airfoil chord length of $R_e = 1.6 \times 10^5$. The numerical results were obtained by Christophe et al. [44] with the solver Ansys Fluent 12, using the k–ω SST model. The numerical results were compared with the available experimental data. As shown in Fig. 11, the pressure coefficient from the RANS simulation is in reasonable agreement with the experimental C_p. The agreement with experiment is much better in the mid-to-late suction side. The boundary layer was analyzed at $x/c = 0.98$ on the suction side, corresponding to remote microphone probe 25 (cf. Fig. 12). The flow data were extracted on a profile normal to the local airfoil surface and are presented in Table 1. This case is critical because the boundary layer is on the verge of separating due to the strong adverse pressure gradient. The shape factor $H = \delta^*/\theta = 2.55$ is typical of such flows. The wall shear stress is obtained by Allen and Tudor's technique [38] and then corrected to obtain $u^+ = y^+$ in the turbulent boundary-layer laminar region.

For the airfoil test cases, the steady flow data are given by the simulations, whereas the wall-pressure fluctuations come from the experimental remote microphone probe measurements.

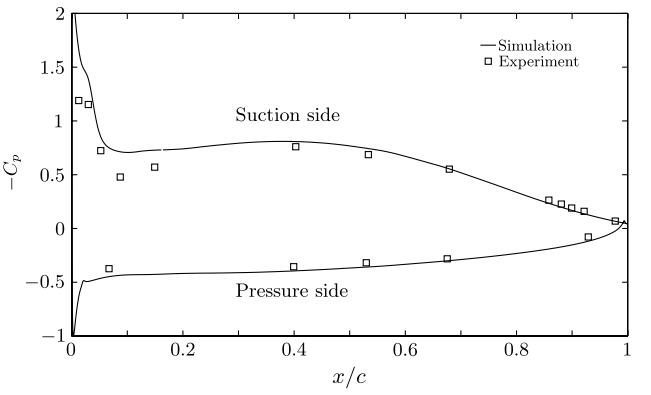

Fig. 11 Mean pressure coefficient ($-C_p$) on CD airfoil.

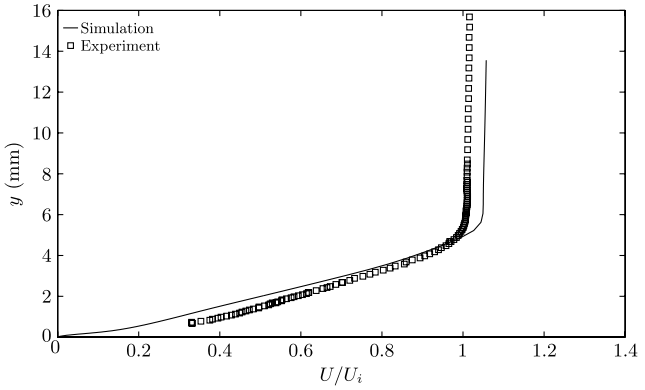

Fig. 12 Mean velocity profile in the boundary layer near the trailing edge (RMP 25).

C. Adverse-Pressure Gradient Markers and Parameters

To build a spectral model able to take into account the adverse pressure gradient effects, we propose in the following section to review the parameters characterizing the pressure-gradient effects and the boundary-layer history. This review will be illustrated by the aforementioned test cases.

In 1956, Coles postulated that the large-eddy structures in the outer layer of the turbulent boundary layer can be represented by a wake profile, with the presence of the wall modifying mainly the viscous sublayer and the logarithm region [45]. The turbulent boundary layer is then described by two functions g and h:

$$u^+ = g(y^+) + \frac{\Pi}{\kappa} h\left(\frac{y}{\delta}\right) \tag{5}$$

where $u^+ = U/u_\tau$, and $y^+ = yu_\tau/\nu$. Π is the wake strength parameter, and the function g is the classical law of the wall:

$$g(y^+) = \frac{1}{\kappa}\ell_n(y^+) + C^+ \tag{6}$$

with $\kappa = 0.41$, the von Kármán constant, and $C^+ = 5.1$. The function h is the law of the wake defined as

$$h\left(\frac{y}{\delta}\right) = 2\sin^2\left(\frac{\pi y}{2\delta}\right) \tag{7}$$

The wake strength parameter Π is found by solving the following equation, derived from the normalization conditions [45]:

$$2\Pi - \ell_n(1+\Pi) = \kappa\frac{U_e}{u_\tau} - \ell_n\left(\frac{\delta^* U_e}{\nu}\right) - \kappa C^+ - \ell_n\kappa \tag{8}$$

Using the results provided by either the experimental or numerical data, the wake strength parameter can be obtained easily. In Fig. 13, velocity profiles in wall units do not follow the law of the wall at high y^+, emphasizing the increase of the wake component. For the considered flows, the wake strength parameter varies between 1.03

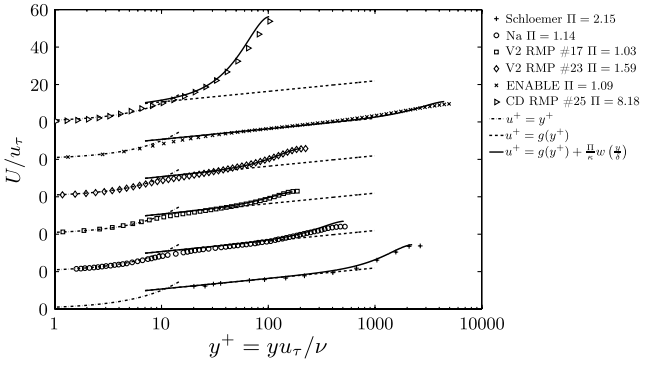

Fig. 13 Velocity profiles in wall units.

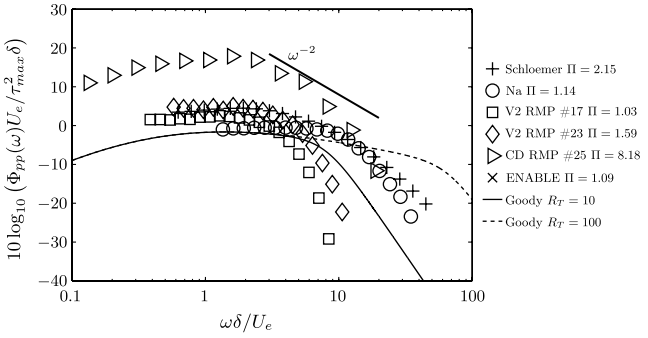

Fig. 14 Wall-pressure spectra normalized by mixed variables using δ. APG spectra compared with Goody's model.

and 2.15, except for the CD airfoil, where its value is much higher with $\Pi = 8.18$, which denotes a boundary layer encountering a very strong adverse pressure gradient. On the suction side of the V2 airfoil, it increases in the adverse pressure gradient region from 1.03 at RMP 17 to 1.59 at RMP 23. The wall-pressure spectra shown in Fig. 14 can be related to the wake strength parameter; the larger Π is, the worse is the agreement between the reference wall-pressure spectra and Goody's model. It emphasizes the need of a wall-pressure spectral model taking into account the effect of the mean pressure gradient.

Velocity profiles experience a growing defect in the near-wall region as the adverse pressure gradient increases. The defect law defined as $(U_e - U)/U_e = f(y/\delta)$ shows large discrepancies for the six profiles in Fig. 15a. To obtain an outer velocity scale and to collapse velocity profiles in the outer region, Zagarola and Smits [46] have proposed a modified defect law. It has been initially developed for a pipe flow and favorably compared to experimental data. Zagarola–Smits's law is defined as $(U_e - U)/U_{ZS} = f(y/\delta)$, where $U_{ZS} = U_e\delta^*/\delta$. Maciel et al. [47] have also applied this defect law to

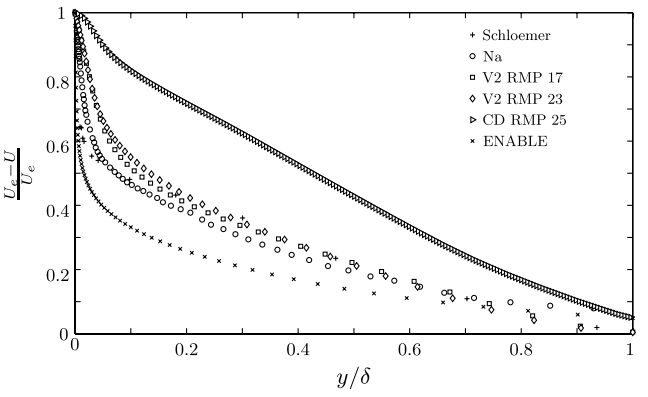

a) Classical defect law

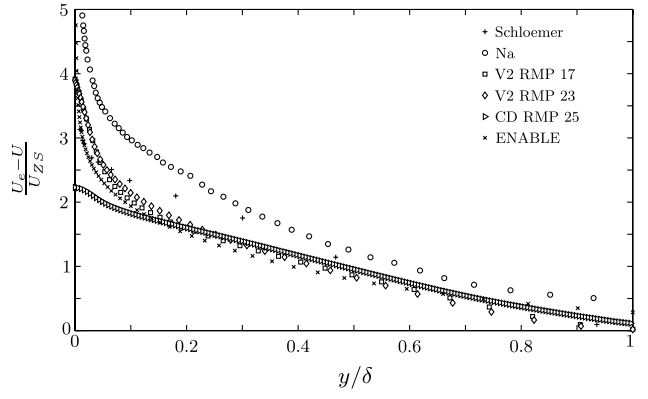

b) Zagarola-Smits' defect law

Fig. 15 Mean velocity in deficit coordinates.

different turbulent boundary layers with APG. Figure 15b shows Zagarola–Smits's defect law for the six velocity profiles. Na and Moin [7] do not provide the boundary-layer thickness δ, and so it has been deduced from the velocity profile, leading to an uncertainty of this quantity. It is not the case for the displacement and momentum thicknesses (δ^* and θ, respectively), in which we are more confident. Zagarola–Smits's defect law provides a better collapse than the classical defect law for the test cases (results by Na excepted). Because it provides an autosimilarity of the velocity profile in the outer region (typically for $y/\delta > 0.2$), $\Delta = \delta/\delta^*$ is then considered as another parameter characterizing the effect of the adverse pressure gradient.

Clauser [48] defined the equilibrium parameter $\beta_C = (\theta/\tau_w)(\mathrm{d}p/\mathrm{d}x)$ to determine whether self-similarity has been achieved. Considering Clauser's definition, the test-case boundary layers are not equilibrium ones. But the pressure gradient parameter β_C is of practical interest to quantify the local pressure gradient and will be used in the next section to develop the empirical spectral model. Whereas both Π and Δ are influenced by the boundary layer history, β_C is rather a local parameter.

IV. Empirical Spectral Model Incorporating Adverse Mean-Pressure Gradient Effects

The use of wall-pressure spectral models, as reviewed in Sec. II, is not relevant to predict wall-pressure spectra of APG flows because it leads to a strong underestimate, especially at low frequencies. Figure 14 illustrates this phenomenon by comparing Goody's model with the APG spectra from the test cases. The discrepancies are important for boundary layers with strong APG, related to high values of Π and β_C. We propose a new model for APG wall-pressure spectra, based on Goody's model including the following corrections:

1) Displacement thickness δ^* is a more-accurate data than the boundary layer thickness δ. The model will be normalized using the mixed variables and δ^* instead of δ.

2) As suggested by Simpson et al. [49], in APG flow, the maximum shearing stress along the normal $\tau_{\max} = \max[\mu(\mathrm{d}U/\mathrm{d}y)]$ has to be preferred to the wall shear stress τ_w to scale the pressure fluctuations.

3) Without any APG, the new model should collapse with Goody's model.

4) In the overlap region of APG flows, the spectral levels decay as $\omega^{-\alpha}$ with α, which can be larger than 0.7 (see the -2 slope in Fig. 14).

5) As $\omega \to \infty$, spectral levels can decay faster than ω^{-5}, especially for the low-Reynolds-number flows. McGrath and Simpson [50] observed a slope -5.5 for $\omega\delta^*/U_e > 7$ (see also Fig. 7 in [51]). When the high-frequency correction (due to the microphone spatial resolution) is significant, the slope at high frequency is difficult to evaluate. The larger correction is obtained for Schloemer's test case, where the attenuation is evaluated to be 9 dB for $\omega\delta^*/U_e = 8$, using the correction proposed by Corcos [16] with an equivalent radius [52] $r_{\mathrm{eq}} = 0.62r$ and a convection velocity $U_c = 0.7U_e$.

6) The global level of fluctuating pressure increases as the pressure gradient parameters increase.

The first correction is applied by rewriting Goody's model with the boundary displacement thickness, assuming a $\frac{1}{7}$th power law for a ZPG. In this particular case, $\Delta = \delta/\delta^* = 8$ and

$$\frac{\Phi_{pp}(\omega)U_e}{\tau_{\max}^2\delta^*} = \frac{C_2'(\omega\delta^*/U_e)^2}{\left[4.76(\omega\delta^*/U_e)^{0.75} + C_1'\right]^{3.7} + [C_3'(\omega\delta^*/U_e)]^7} \tag{9}$$

with $C_1' = 0.5$, $C_2' = 1536$, and $C_3' = 8.8R_T^{-0.57}$.

Based on the new formulation of Goody's model using the displacement thickness [Eq. (9)], the derived functional form is

$$\frac{\Phi_{pp}(\omega)U_e}{\tau_{\max}^2\delta^*} = \frac{F_2(\Pi,\beta_C,\Delta)(\omega\delta^*/U_e)^2}{\left[4.76(\omega\delta^*/U_e)^{0.75} + F_1(\Pi,\beta_C,\Delta)\right]^{A1} + [C_3'(\omega\delta^*/U_e)]^{A_2}} \tag{10}$$

First, the coefficients A_1 and A_2 that drive the slope, respectively, in the overlap and in the high frequency regions are deduced to meet the previous requirements, leading to

$$A_1 = 3.7 + 1.5\beta_C, \qquad A_2 = \min(3, 19/\sqrt{R_T}) + 7$$

F_1 is then determined so that $(\Phi_{pp}(\omega)U_e)/[\tau_{\max}^2\delta^* F_2(\Pi,\beta_C,\Delta)]$ is maximum for $\omega\delta/U_e = 1.4$ or equivalently for $\omega\delta^*/U_e = 1.4/\Delta$, as in Goody's model. A fairly accurate approximation is given by

$$F_1 = 4.76\left(\frac{1.4}{\Delta}\right)^{0.75}[0.375A_1 - 1] \tag{11}$$

$F_2 = F_{2a}.F_{2b}$ is then determined by a two-step procedure. First, F_{2a} is calculated to satisfy $\{10\log_{10}[(\Phi_{pp}(\omega)U_e)/(\tau_{\max}^2\delta^*)]\}_{\max} \approx$ 7.4 dB for $\omega\delta/U_e = 1.4$, assuming $F_{2b} = 1$. It assures for a zero pressure gradient spectrum to behave as Goody's model at low frequencies. Then, $F_{2b} = 4.2\left(\Pi/\Delta\right) + 1$ has been determined thanks to the six reference spectra presented in Sec. III.B. As the APG increases, Π increases and Δ decreases, hence the idea to combine these effects and to define the variable Π/Δ.

The final proposed model is then fully determined by

$$\frac{\Phi_{pp}(\omega)U_e}{\tau_{\max}^2\delta^*} = \frac{\left[2.82\Delta^2(6.13\Delta^{-0.75} + F_1)^{A1}\right][4.2\left(\frac{\Pi}{\Delta}\right) + 1]\tilde{\omega}^2}{[4.76\tilde{\omega}^{0.75} + F_1]^{A1} + [C_3'\tilde{\omega}]^{A2}} \tag{12}$$

Figure 16 shows how the model behaves as the pressure gradient parameters vary. As Δ decreases, with Π and β_C being held constants at nonzero values, the level of the normalized pressure spectrum is increased at mid and high frequencies whereas it decreases at low frequencies (cf. Fig. 16a. In Fig. 16b, Δ is held constant as β_C increases. β_C and Π are correlated and cannot vary independently. Durbin and Reif [53] proposed the following empirical formula:

$$\Pi = 0.8(\beta_C + 0.5)^{3/4} \tag{13}$$

which is used to calculate Π in Fig. 16b. As Π and β_C increase, the maximum obtained at $\omega\delta^*/U_e = 1.4/\Delta$ is higher, and the overlap region is decreased.

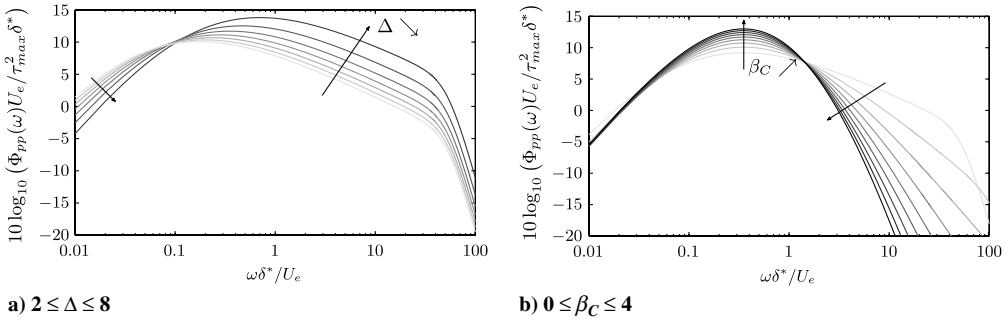

a) $2 \le \Delta \le 8$ **b) $0 \le \beta_C \le 4$**

Fig. 16 Evolution of the wall-pressure spectral model with the adverse pressure gradient parameters.

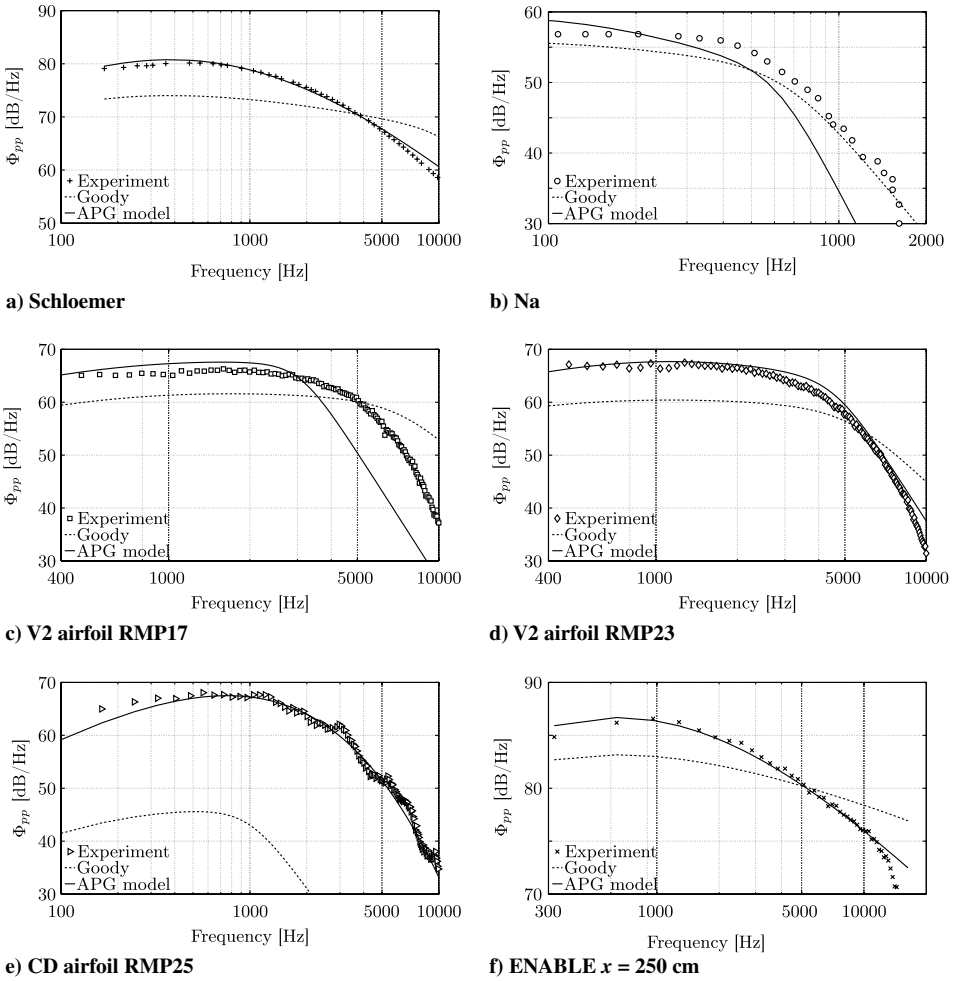

Fig. 17 Wall-pressure spectra. Comparison between Goody's model and present model.

V. Results

The model for APG wall-pressure spectra is compared to the reference spectra in Fig. 17. The new model is in better agreement than Goody's model, which is an expected result because Goody's model is only valid for ZPG boundary layers. The agreement is poorer for flows with a mild pressure gradient (cf. Figs. 17b and 17c).

Knowing the wall-pressure spectrum in the vicinity of the trailing edge and assuming an attached flow, the noise radiated as boundary layer vorticity is convected past the trailing edge of an airfoil and can be predicted using analytical models [1,3]. The coherence length scale l_y and the convection velocity U_c have also to be determined to predict the radiated noise using Amiet's model [1]. The sound radiated in the midspan plane by the CD airfoil has been measured by Moreau and Roger [34]. The microphone is placed at a distance $R = 2$ m above the airfoil trailing edge ($\theta = 90$ deg). The results are presented in Fig. 18. At low and high frequencies, the signal-to-noise ratio is very low, and the experimental data are limited to the range [200 Hz–2 kHz]. To predict the far-field noise analytically, the coherence length scale is determined by Corcos's model:

$$ly(\omega) = \frac{bU_c}{\omega} \tag{14}$$

with $U_c = 0.7U_i$ and $b = 1.47$, determined by postprocessing experimental results [34]. For a loaded airfoil, the far-field pressure is strongly related to the wall-pressure spectrum in the vicinity of the trailing edge on the suction side. Amiet's model strongly underestimates the far field spectra if wall-pressure spectra is

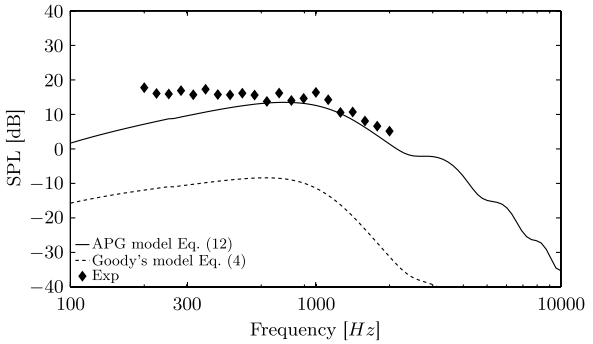

Fig. 18 Far-field acoustic spectra in the midspan plane above the CD airfoil at a distance of 2 m. Experiment from Moreau and Roger [34] is compared to Amiet's model.

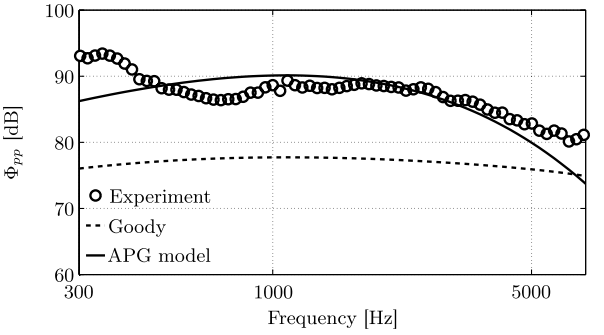

Fig. 19 Wall-pressure spectrum in the aft region of a NACA5510 profile. Comparison between Goody's model and present model.

Table 2 Inner and outer boundary-layer variables on Brooks and Hodgson's NACA 0012; results from XFOIL 6.9

Distance upstream of TE	U_e, m/s	δ, m	δ^*, m	θ, m	H	τ_w, Pa	β_C	Π	R_θ	Δ
$x_{\mathrm{TE}} = 18$ mm	64.6	1.42×10^{-2}	2.36×10^{-3}	1.57×10^{-3}	1.49	5.43	3.51	1.56	6747	6.00
$x_{\mathrm{TE}} = 77$ mm	69.3	0.97×10^{-2}	1.62×10^{-3}	1.12×10^{-3}	1.43	8.52	0.60	0.56	5145	6.00

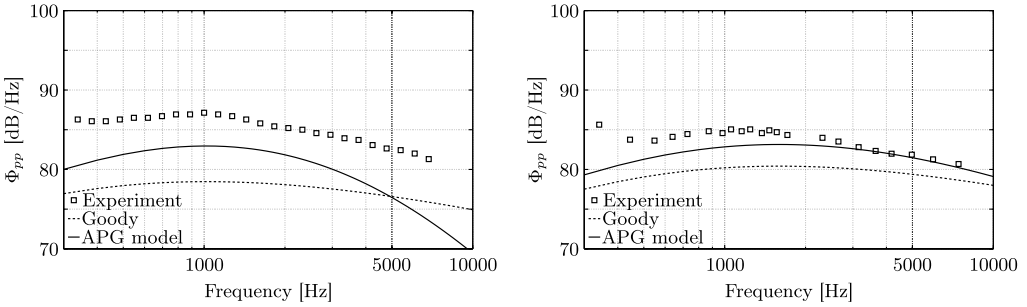

a) 1.85 cm upstream of TE **b) 7.72 cm upstream of TE**

Fig. 20 NACA0012 wall-pressure spectra. Goody's model, present model, and experiments by Brooks and Hodgson [56].

determined using Goody's model. With the new model for APG flows, the agreement is much better.

To demonstrate the ability of the model to predict the wall-pressure spectrum of any flow encountering APG, it is evaluated on two demonstration cases not connected to the database. For the first case, the experimental data have been carried out in the anechoic wind tunnel at ECL. A NACA5510 profile with a 200 mm chord and a 200 mm span is placed into the core of a jet at a reference velocity of 70 m/s. The angle of attack is 15 deg, and we will focus on the results in the aft region of the suction side, where the pressure gradient is positive ($x/c = 95\%$). More details on the experimental setup are given by Jacob et al. [54]. This configuration has been numerically studied by Boudet et al. [55], following a classical RANS approach. The results of the numerical simulation are used as input data for the model, and the comparison of the wall-pressure spectrum at midspan near the trailing edge is presented in Fig. 19. The APG model is in better agreement with the experimental data than Goody's model.

The second demonstration case is the well-known NACA0012 experiment by Brooks and Hodgson [56]. The configuration with an angle of attack of 0 deg at 69.5 m/s with a sharp trailing edge is studied. This configuration enables the boundary-layer parameters to be estimated by neglecting the installation effect. Thus, XFOIL 6.9 is used to provide boundary-layer displacement and momentum thicknesses, friction coefficient, external velocity, and pressure distribution. The boundary-layer thicknesses ratio ($\Delta = \delta/\delta^*$) is given by the experimental data of Garcia-Sagrado et al. [57] on the same airfoil at a lower Reynolds number. Boundary-layer parameters are summarized in Table 2. Figure 20 compares the experimental wall-pressure spectra to Goody's and present models for two chordwise positions upstream of the trailing edge. For both locations, 1.8 and 7.7 cm upstream of the trailing edge ($x/c = 97\%$ and 87%, respectively), Goody's model underestimates pressure level of about 7 and 4 dB, respectively. The APG model improves the prediction but is still lower than the experimental data. At 7.7 cm upstream of the trailing edge, the APG model is less than 2 dB below the experimental result and, at 1.8 cm upstream of the trailing edge, it is between 3 and 5 dB below. The wall-pressure spectrum prediction is then improved by the APG model. Figure 21 shows that the use of the APG model improves the trailing-edge noise prediction based on Amiet's theory.

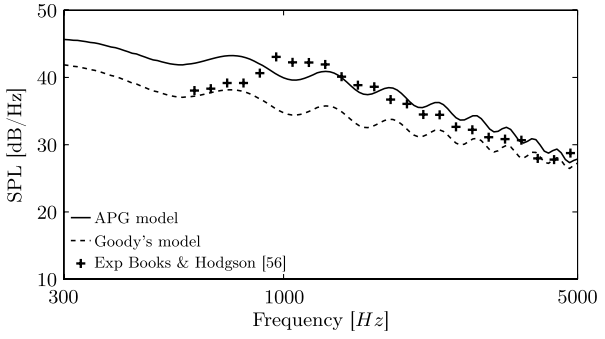

Fig. 21 Far-field acoustic spectrum in the midspan plane at a distance $R = 1.2$ m above a NACA 0012 at $U_0 = 69.5$ m/s.

VI. Conclusions

An extension of Goody's model enabling the prediction of adverse pressure gradient (APG) wall-pressure spectrum was developed and assessed on the basis of six test cases. The model requires the knowledge of the mean steady flowfield, more precisely the streamwise pressure distribution and the velocity profile normal to the wall, given by a Reynolds-averaged Navier–Stokes (RANS) simulation for instance. It is demonstrated that the effect of APG cannot be neglected because it leads to an underestimate of the wall-pressure spectrum directly affecting the far-field noise prediction when applied to the trailing-edge noise prediction. It is proposed that the more relevant parameters that drive the effects of the pressure gradient on the turbulent boundary layer are the wake strength parameter, Clauser's parameter, and the ratio of the boundary layer to displacement thicknesses. The APG model can be used for flows on the verge of separating, as long as they remain attached. It improves the pressure level prediction and the shape of the spectra, especially for high-pressure gradient flows.

Only a few studies have been published on APG flows in which both mean flowfield and wall-pressure fluctuations are provided. Further validation would benefit from new test cases. Comparison to data for three-dimensional boundary layers are also warranted. It should also be noted that the model is limited to APG flows and cannot be applied to favorable pressure gradient flows.

The model can be used as postprocessing of RANS simulations, which are affordable in industrial context for complex geometries. It is almost instantaneous, and the total (RANS and postprocessing) computational costs are small compared with a large-eddy simulation. It can be coupled with analytical approaches to predict airfoil trailing-edge noise. The coupling with the extended Amiet's model to rotating blade would be an interesting study, especially for the prediction of wind turbine noise.

Acknowledgments

The authors would like to thank Douglas Neal, who carried out the hot-wire measurements on the controlled-diffusion airfoil at Michigan State University, and Julien Christophe, who provided the

Reynolds-averaged Navier–Stokes (RANS) simulation on the controlled-diffusion airfoil at the von Karman Institute.

The data on the NACA5510 airfoil have been obtained in the framework of the EU project PROBAND–Improvement of Fan Broadband Noise Prediction: Experimental Investigation and Computational Modelling. The authors would like to thank Marc Jacob and Julien Grilliat for the experimental results as well as Joëlle Caro for the RANS simulation.

References

[1] Amiet, R. K., "Noise Due to Turbulent Flow Past a Trailing Edge," *Journal of Sound and Vibration*, Vol. 47, No. 3, 1976, pp. 387–393. doi:10.1016/0022-460X(76)90948-2

[2] Howe, M. S., "A Review of the Theory of Trailing-Edge Noise," *Journal of Sound and Vibration*, Vol. 61, No. 3, 1978, pp. 437–465. doi:10.1016/0022-460X(78)90391-7

[3] Howe, M. S., "Edge-source Acoustic Green's Function for an Airfoil of Arbitrary Chord, with Application to Trailing-Edge Noise," *Quarterly Journal of Mechanics and Applied Mathematics*, Vol. 54, No. 1, 2001, pp. 139–155. doi:10.1093/qjmam/54.1.139

[4] Roger, M., and Moreau, S., "Back-Scattering Correction and Further Extensions of Amiet's Trailing Edge Noise Model. Part 1: Theory," *Journal of Sound and Vibration*, Vol. 286, No. 3, 2005, pp. 477–506. doi:10.1016/j.jsv.2004.10.054

[5] Bull, M. K., "Wall-Pressure Fluctuations Beneath Turbulent Boundary Layers: Some Reflections on Forty Years of Research," *Journal of Sound and Vibration*, Vol. 190, No. 3, 1996, pp. 299–315. doi:10.1006/jsvi.1996.0066

[6] Choi, H., and Moin, P., "On the Space-Time Characteristics of Wall-Pressure Fluctuations," *Physics of Fluids A*, Vol. 2, No. 8, 1990, pp. 1450–1460. doi:10.1063/1.857593

[7] Na, Y., and Moin, P., "The Structure of Wall-Pressure Fluctuations in Turbulent Boundary Layers with Adverse Pressure Gradient and Separation," *Journal of Fluid Mechanics*, Vol. 377, 1998, pp. 347–373. doi:10.1017/S0022112098003218

[8] Sandberg, R., and Sandham, N., "Direct Numerical Simulations of Turbulent Flow Past a Trailing Edge and the Associated Noise Generation," *Journal of Fluid Mechanics*, Vol. 596, 2008, pp. 353–385. doi:10.1017/S0022112007009561

[9] Lee, Y. T., Blake, W. K., and Farabee, T. M., "Modeling of Wall Pressure Fluctuations Based on Time Mean Flow Field," *Journal of Fluids Engineering*, Vol. 127, No. 2, 2005, pp. 233–240. doi:10.1115/1.1881698

[10] Lee, Y. T., Farabee, T. M., and Blake, W. K., "Turbulence Effects of Wall-Pressure Fluctuations for Reattached Flow," *Computers and Fluids*, Vol. 38, 2009, pp. 1033–1041. doi:10.1016/j.compfluid.2008.01.012

[11] Peltier, L. J., and Hambric, S. A., "Estimating Turbulent Boundary Layer Wall-Pressure Spectra from CFD RANS Solutions," *Journal of Fluids and Structures*, Vol. 23, 2007, pp. 920–937. doi:10.1016/j.jfluidstructs.2007.01.003

[12] Remmler, S., Christophe, J., Anthoine, J., and Moreau, S., "Computation of Wall-Pressure Spectra from Steady Flow Data for Noise Prediction," *AIAA Journal*, Vol. 48, No. 9, 2010, pp. 1997–2007. doi:10.2514/1.J050206

[13] Panton, R. L., and Linebarger, J. H., "Wall Pressure Spectra Calculations for Equilibrium Boundary Layers," *Journal of Fluid Mechanics*, Vol. 65, No. 2, 1974, pp. 261–287. doi:10.1017/S0022112074001388

[14] Goody, M., "Empirical Spectral Model of Surface Pressure Fluctuations," *AIAA Journal*, Vol. 42, No. 9, 2004, pp. 1788–1794. doi:10.2514/1.9433

[15] Keith, W. L., Hurdis, D. A., and Abraham, B. M., "A Comparison of Turbulent Boundary Layer Wall-Pressure Spectra," *Journal of Fluids Engineering*, Vol. 114, No. 3, 1992, pp. 338–347. doi:10.1115/1.2910035

[16] Corcos, G. M., "Resolution of Pressure in Turbulence," *Journal of the Acoustical Society of America*, Vol. 35, No. 2, 1963, pp. 192–199. doi:10.1121/1.1918431

[17] Hwang, Y. F., Bonness, W. K., and Hambric, A., "Comparison of Semi-Empirical Models for Turbulent Boundary Layer Wall Pressure Spectra," *Journal of Sound and Vibration*, Vol. 319, 2009, pp. 199–217. doi:10.1016/j.jsv.2008.06.002

[18] Willmarth, W. W., and Roos, F. W., "Resolution and Structure of the Wall Pressure Field Beneath a Turbulent Boundary Layer," *Journal of Fluid Mechanics*, Vol. 22, 1965, pp. 81–94. doi:10.1017/S0022112065000599

[19] Bakewell, H. P., Carey, G. F., Libuha, J. J., Schloemer, H. H., and Von Winkle, W. A., "Wall Pressure Correlations in Turbulent Pipe," Underwater Sound Laboratory TR 559, 1962.

[20] Bull, M. K., "Wall-Pressure Fluctuations Associated with Subsonic Turbulent Boundary Layer Flow," *Journal of Fluid Mechanics*, Vol. 28, No. 4, 1967, pp. 719–754. doi:10.1017/S0022112067002411

[21] Bull, M. K., and Thomas, S. W., "High Frequency Wall Pressure Fluctuations in Turbulent Boundary Layers," *Physics of Fluids*, Vol. 19, No. 4, 1976, pp. 597–599. doi:10.1063/1.861496

[22] Carey, G. F., Chlupsa, J. E., and Schloemer, H. H., "Acoustic Turbulent Water-Flow Tunnel," *Journal of the Acoustical Society of America*, Vol. 41, No. 2, 1967, pp. 373–379. doi:10.1121/1.1910348

[23] Farabee, T. M., "An Experimental Investigation of Wall Pressure Fluctuations Beneath Non-Equilibrium Turbulent Flows," David Taylor Naval Ship Research and Development Center TR 86/047, 1986.

[24] Keith, W. L., and Bennett, J. C., "Low Frequency Measurements of the Wall Shear Stress and Wall Pressure in a Turbulent Boundary Layer," *AIAA Journal*, Vol. 29, No. 4, 1991, pp. 526–530. doi:10.2514/3.10615

[25] Schewe, G., "On the Structure and Resolution of Wall-Pressure Fluctuations Associated with Turbulent Boundary-Layer Flow," *Journal of Fluid Mechanics*, Vol. 134, 1983, pp. 311–328. doi:10.1017/S0022112083003389

[26] Schloemer, H. H., "Effects of Pressure Gradients on Turbulent-Boundary-Layer Wall-Pressure Fluctuations," *Journal of the Acoustical Society of America*, Vol. 42, No. 1, 1967, pp. 93–113. doi:10.1121/1.1910581

[27] Willmarth, W.W, and Wooldridge, C. E., "Measurements of the Fluctuating Pressure at the Wall Beneath a Thick Turbulent Boundary Layer," *Journal of Fluid Mechanics*, Vol. 14, 1962, pp. 187–210. doi:10.1017/S0022112062001160

[28] Chase, D. M., "Modeling the Wavevector-Frequency Spectrum of Turbulent Boundary Layer Wall Pressure," *Journal of Sound and Vibration*, Vol. 70, No. 1, 1980, pp. 29–67. doi:10.1016/0022-460X(80)90553-2

[29] Howe, M. S., *Acoustics of Fluid-Structure Interactions*, Cambridge Univ. Press, New York, 1998, pp. 204–209.

[30] Bradshaw, P., "'Inactive' Motion and Pressure Fluctuations in Turbulent Boundary Layers," *Journal of Fluid Mechanics*, Vol. 30, No. 2, 1958, pp. 241–258. doi:10.1017/S0022112067001417

[31] Na, Y., "Direct Numerical Simulation of Turbulent Boundary Layers with Adverse Pressure Gradient and Separation," Ph.D. Dissertation, Stanford Univ., Stanford, CA, 1996.

[32] Robert, G., "Experimental Database for the Pressure Gradient Effect," European Union Research Programme TR G4RD-CT-2000-00223, 2002.

[33] Rozenberg, Y., Roger, M., and Moreau, S., "Effect of Blade Design at Equal Loading on Broadband Noise," 12th AIAA/CEAS Aeroacoustics Conference, Cambridge, MA, AIAA Paper 2006-2563, May 2006.

[34] Moreau, S., and Roger, M., "Effect of Airfoil Aerodynamic Loading on Trailing-Edge Noise Sources," *AIAA Journal*, Vol. 43, No. 1, 2005, pp. 41–52. doi:10.2514/1.5578

[35] Spalart, P. R., and Watmuff, J. H., "Experimental and Numerical Study of a Turbulent Boundary Layer with Pressure Gradients," *Journal of Fluid Mechanics*, Vol. 249, 1993, pp. 337–371. doi:10.1017/S002211209300120X

[36] Patel, V. C., "Calibration of the Preston Tube and Limitations on Its Use in Pressure Gradients," *Journal of Fluid Mechanics*, Vol. 23, 1965, pp. 185–208. doi:10.1017/S0022112065001301

[37] Klebanoff, P. S., "Characteristics of Turbulence in a Boundary Layer with Zero Pressure Gradient," NACA, TR 1247, 1955.

[38] Allen, J. M., and Tudor, D. H., "Charts for Interpolation of Local Skin Friction From Experimental Turbulent Velocity Profiles," NASA SP 3048, 1969.

[39] Moreau, S., and Roger, M., "Back-Scattering Correction and Further Extensions of Amiet's Trailing Edge Noise Model. Part 2: Application," *Journal of Sound and Vibration*, Vol. 323, 2009, pp. 397–425. doi:10.1016/j.jsv.2008.11.051

[40] Perennès, S., and Roger, M., "Aerodynamic Noise of a Two-Dimensional Wing with Highlift Devices," 4th AIAA/CEAS Aeroacoustics Conference Meeting, Toulouse, France, AIAA

Paper 1998-2338, June 1998.
[41] Moreau, S., Henner, M., Iaccarino, G., Wang, M., and Roger, M., "Analysis of Flow Conditions in Freejet Experiments for Studying Airfoil Self-Noise," *AIAA Journal*, Vol. 41, No. 10, 2003, pp. 1895–1905.
doi:10.2514/2.1905
[42] Menter, F. R., "Two-Equation Eddy-Viscosity Turbulence Models for Engineering Applications," *AIAA Journal*, Vol. 32, No. 8, 1994, pp. 1598–1605.
doi:10.2514/3.12149
[43] Wang, M., Moreau, S., Iaccarino, G., and Roger, M., "LES Prediction of Wall-Pressure Fluctuations and Noise of a Low-Speed Airfoil," *International Journal of Aeroacoustics*, Vol. 8, No. 3, 2009, pp. 177–197.
doi:10.1260/147547208786940017
[44] Christophe, J., Moreau, S., Hamman, C. W., Witteveen, J. A. S., and Iaccarino, G., "Uncertainty Quantification for Trailing-Edge Noise of a Controlled-Diffusion Airfoil," *Center for Turbulence Research, Proceedings of the Summer Program 2010*, 2010.
[45] Coles, D., "The Law of the Wake in the Turbulent Boundary Layer," *Journal of Fluid Mechanics*, Vol. 1, No. 2, 1956, pp. 191–226.
doi:10.1017/S0022112056000135
[46] Zagarola, M. V., and Smits, A. J., "Mean-Flow Scaling of Turbulent Pipe Flow," *Journal of Fluid Mechanics*, Vol. 373, 1998, pp. 33–79.
doi:10.1017/S0022112098002419
[47] Maciel, Y., Rossignol, K.-S., and Lemay, J., "Self-Similarity in the Outer Region of Adverse-Pressure- Gradient Turbulent Boundary Layers," *AIAA Journal*, Vol. 44, No. 11, 2006, pp. 2450–2464.
doi:10.2514/1.19234
[48] Clauser, F. H., "Turbulent Boundary Layers in Adverse Pressure Gradients," *Journal of the Aeronautical Sciences*, Vol. 21, No. 2, 1954, pp. 91–108.
[49] Simpson, R. L., Ghodbane, M., and McGrath, B. E., "Surface Pressure Fluctuations in a Separating Turbulent Boundary Layer," *Journal of Fluid Mechanics*, Vol. 177, 1987, pp. 167–186.
doi:10.1017/S0022112087000909
[50] McGrath, B. E., and Simpson, R. L., "Some Features of Surface Pressure Fluctuations in Turbulent Boundary Layers with Zero and Favorable Pressure Gradients," NASA CR 4051, 1987.
[51] Goody, M., and Simpson, R. L., "Surface Pressure Fluctuations Beneath Two- and Three-Dimensional Turbulent Boundary Layers," *AIAA Journal*, Vol. 38, No. 10, 2000, pp. 1822–1831.
doi:10.2514/2.863
[52] Gilchrist, R. B., and Strawderman, W. A., "Experimental Hydrophone-Size Correction Factor for Boundary-Layer Pressure Fluctuations," *Journal of the Acoustical Society of America*, Vol. 38, 1965, pp. 298–302.
doi:10.1121/1.1909663
[53] Durbin, P. A., and Reif, B. A. P., *Statistical Theory and Modeling for Turbulent Flows*, Wiley, New York, 2001, p. 68.
[54] Jacob, M. C., Grilliat, J., Camussi, R., and Caputi-Genaro, G., "Aeroacoustic Investigation of a Single Airfoil Tip Leakage Flow," *International Journal of Aeroacoustics*, Vol. 9, No. 3, 2010, pp. 253–272.
doi:10.1260/1475-472X.9.3.253
[55] Boudet, J., Grilliat, J., Caro, J., and Jacob, M. C., "Combined Experimental/Computational Study of Tip Clearance Flow and Acoustics," *European Turbomachinery Conference*, 2009.
[56] Brooks, T. F., and Hodgson, T. H., "Trailing Edge Noise Prediction from Measured Surface Pressures," *Journal of Sound and Vibration*, Vol. 78, No. 1, 1981, pp. 69–117.
doi:10.1016/S0022-460X(81)80158-7
[57] Garcia-Sagrado, A., Hynes, T., and Hodson, H., "Experimental Investigation into Trailing Edge Noise Sources," Proceedings of the 12th AIAA/CEAS Aeroacoustics Conference, Cambridge, MA, AIAA Paper 2006-2476, 2006.

A. Lyrintzis
Associate Editor